Title	The use of a dynamic truck-trailer drive-by system to monitor bridge damping
Authors(s)	Keenahan, Jennifer; O'Brien, Eugene J.; McGetrick, P.; González, Arturo
Publication date	2013-12
Publication information	Structural Health Monitoring, 13 (2): 143-157
Publisher	Sage Publications
Item record/more information	http://hdl.handle.net/10197/6240
Publisher's version (DOI)	10.1177/1475921713513974

Introduction

Traditionally, the task of detecting damage in bridges consists of visual inspections, which are labour intensive and are often an unreliable way of determining the true condition. With the increase in computational power and signal processing capacity, there has been a move towards sensor based analysis of bridge condition. Vibration based approaches are based on the assumption that changes in the physical properties of a structure (stiffness, mass and energy dissipation mechanisms) cause changes in the modal properties (frequency, damping and mode shapes). For example, a change in the stiffness of a bridge (indicating that it may be damaged) can be detected by a change in its natural frequencies. Changing environmental conditions may be accounted for by heating and cooling correction factors determined from surface temperature measurement in the field. Existing monitoring techniques generally involve the direct instrumentation of the structure – commonly referred to as Structural Health Monitoring (SHM).[1–3] However, monitoring via direct instrumentation only would require the installation and maintenance of sensors and data acquisition electronics on the entire bridge stock which would be expensive and time consuming. More recently, a small number of authors have shifted to the instrumentation of a vehicle, rather than the bridge, in order to assess bridge condition. This approach, referred to as 'drive-by' bridge inspection[4], has potential advantages in terms of reduced cost and ease of implementation.

With sensors on the structure, many researchers use natural frequencies as damage detection mechanisms, which can be measured inexpensively and with relative ease.[5,6] The feasibility of detecting frequencies from the dynamic response of an instrumented vehicle passing over a bridge has been verified theoretically by Yang et al.[7] This method was later tested in field trials.[8,9] Laboratory investigations have also been conducted to check the feasibility of the approach as part of a drive-by inspection system for bridge monitoring.[4,10–12] It should be noted however, that using frequency shifts to detect damage has practical limitations, especially in the case of large structures.[13] A numerical and experimental study by González et al.[14] analyses a 3D Finite Element (FE) Vehicle-Bridge Interaction (VBI) model and they

conclude that accurate determination of the bridge frequency from the vehicle response is only feasible for low velocities and high dynamic excitation of the bridge.

As an alternative to detecting changes in frequency, Yabe & Miyamoto[15] use the mean displacement of the rear axle of a city bus passing over a bridge a large number of times as a damage indicator. Kim et al.[16] construct scaled VBI laboratory experiments and consider the use of autoregressive coefficients as a damage indicator. The analysis of damping has been considered to a lesser extent in the field of damage detection,[17] however, it is one of a number of possible indicators which might be used alone or in combinaton with other indicators (such as mode shapes or frequency changes). While a definitive link between changes in damping and the occurrence of damage is by no means proven, recent evidence suggests that damping is quite sensitive to damage in structural elements and in some cases, more sensitive than natural frequencies. Wahab & De Roeck[18] note that the additional surfaces created by new cracks tend to increase damping ratios. Curadelli et al.[13] show that when cracks occur there is little or no frequency variation but that changes in damping may be used to detect the nonlinear dissipative effects that cracks produce. Modena et al.[19] show that visibly undetectable cracks cause very little change in resonant frequencies and require higher mode shapes to be detected, while these same cracks cause significant changes in damping. In some cases, damping changes of around 50% are observed. Gutenbrunner et al.[20] artificially introduce structural damage in a pre-stressed concrete bridge by eliminating some of the tendons and note that the damping ratio changes from 1.19% to 2.21% due to the removal of these tendons. Further, many researchers note that damping can be a useful damage sensitive feature and is highly indicative of the amount of damage that a structure has undergone during its lifetime.[21,22]

This paper assesses the feasibility of drive-by damage detection using a numerical model of vehicle-bridge dynamic interaction. Some authors have modelled the vehicle as a single vertical force or as a series of constant forces.[23–25] Others have modelled the vehicle as a lumped sprung mass model[7,26–28] or a

train as a series of sprung masses lumped at the bogie positions.[29] A slightly more comprehensive vehicle model is the two-degree-of-freedom (vehicle body bounce and axle hop) quarter-car used by many authors.[30–34] Body pitching motions are taken into account of in the four-degree-of-freedom half-car.[30,35–37] Some authors have extended this further and have modelled an articulated truck.[38–42] Others have created numerical models of real world vehicles – such as the Ford Cargo truck, the Isuzu dump truck[36] and the AASHTO HS20-44 truck.[43]

This paper describes a numerical study of a novel approach that uses a truck-trailer vehicle system, fitted with accelerometers on the trailer axles, to detect changes in the damping of a bridge which would indicate deterioration of the bridge's condition. The concept is that the relatively heavy truck dynamically excites the bridge while sensors in the trailer, with a simpler suspension system, are used to monitor the resulting vibrations. For numerical simulations, a VBI model is created in Matlab. The vehicle model consists of a three axle, five-degree-of-freedom non-articulated truck towing a two axle, four-degree-of freedom trailer. An FE beam model represents the bridge. The trailer axles are assigned identical properties – as can easily be the case with a simple trailer. The axle accelerations from the front and rear axles of the trailer are *subtracted* from one another. Each trailer axle is excited by the same road profile and by an element of bridge vibration at a different point in time. Subtracting the signals, time shifted by the interval between axle arrivals, has the effect of removing most of the influence of the road profile. This is a key feature of this approach and is the reason why the results are better than in simpler single-axle drive-by monitoring concepts.

Vehicle-bridge interaction model

VBI is modelled here as a coupled system, so the solution is given at each time step and no iteration is required in the computational process. The bridge and vehicle models are outlined in the following sections.

Bridge model

The bridge model used here is a simply supported 15 m FE beam that consists of twenty discretized beam elements with four degrees of freedom. The beam therefore has a total of $n = 42$ degrees of freedom. It has a constant modulus of elasticity $E = 3.5 \times 10^{10}$ N m^{-2}, mass per unit length, $\mu = 28\ 125$ kg m^{-1} and second moment of area, $J = 0.5273$ m^4. The first natural frequency of the beam is 5.65 Hz. The response of a discretized beam model to a series of moving time-varying forces is given by the system of equations:

$$\mathbf{M_b}\ddot{\mathbf{y}}_\mathbf{b} + \mathbf{C_b}\dot{\mathbf{y}}_\mathbf{b} + \mathbf{K_b}\mathbf{y_b} = \mathbf{N_b}\mathbf{f_{int}} \quad (1)$$

where $\mathbf{M_b}$, $\mathbf{C_b}$ and $\mathbf{K_b}$ are the ($n \times n$) global mass, damping and stiffness matrices of the beam model respectively and $\mathbf{y_b}$, $\dot{\mathbf{y}}_\mathbf{b}$ and $\ddot{\mathbf{y}}_\mathbf{b}$ are the ($n \times 1$) global vectors of nodal bridge displacements and rotations, their velocities and accelerations respectively. The product $\mathbf{N_b}\mathbf{f_{int}}$ is the ($n \times 1$) global vector of forces applied to the bridge nodes. The vector $\mathbf{f_{int}}$ contains the interaction forces between the vehicle and the bridge and is described using the following vector:

$$\mathbf{f_{int}} = \mathbf{P} + \mathbf{F_t} \quad (2)$$

where $\mathbf{P}$ is the static axle load vector and the vector $\mathbf{F_t}$ contains the dynamic wheel contact forces of each axle. The matrix $\mathbf{N_b}$ is a ($n \times n_f$) location matrix that distributes the n_f applied interaction forces on beam elements to equivalent forces acting on nodes. This location matrix can be used to calculated bridge displacement under each wheel, $\mathbf{y_{br}}$:

$$\mathbf{y_{br}} = \mathbf{N_b^T}\,\mathbf{y_b} \quad (3)$$

The damping ratio of the bridge, ξ, is varied in simulations to assess the system's potential as an indicator of changes in damping. Although complex damping mechanisms may be present in the structure, viscous damping is typically used for bridge structures and deemed to be sufficient to reproduce the bridge response accurately. Therefore, Rayleigh damping is adopted here to model viscous damping:

$$\mathbf{C_b} = \alpha\mathbf{M_b} + \beta\mathbf{K_b} \quad (4)$$

where α and β are constants. The damping ratio is assumed to be the same for the first two modes[44] and α and β are obtained from $\alpha = 2\,\xi\,\omega_1\omega_2/(\omega_1+\omega_2)$ and $\beta = 2\,\xi\,/\,(\omega_1+\omega_2)$ where ω_1 and ω_2 are the first two natural frequencies of the bridge.[45] For comparison, a hysteresis damping model is also used, and the results are present in the section titled '*Hysteresis damping – an alternative model to rayleigh damping*'.

Vehicle model

Two vehicle models are used in this paper. The first is a system of two quarter-cars to illustrate the concept of subtracting axle accelerations, the second is the truck-trailer model. The equations of motion of the vehicle models are obtained by imposing equilibrium of all forces and moments acting on the vehicle and expressing them in terms of the degrees of freedom. They are given by

$$\mathbf{M_v}\ddot{\mathbf{y}}_\mathbf{v} + \mathbf{C_v}\dot{\mathbf{y}}_\mathbf{v} + \mathbf{K_v}\mathbf{y_v} = \mathbf{f_v} \tag{5}$$

where $\mathbf{M_v}$, $\mathbf{C_v}$ and $\mathbf{K_v}$ are the mass, damping and stiffness matrices of the vehicle respectively. $\mathbf{y_v}$, $\dot{\mathbf{y}}_\mathbf{v}$ and $\ddot{\mathbf{y}}_\mathbf{v}$ are the ($n \times 1$) vectors of vehicle displacements, their velocities and accelerations respectively. $\mathbf{f_v}$ is the time varying interaction force vector applied to the vehicle.

The dynamic interaction between the vehicle and the bridge is implemented in Matlab. The vehicle and the bridge are coupled at the tyre contact points via the interaction force vector, $\mathbf{f_{int}}$. Combining equation (1) and equation (5), the coupled equation of motion is formed as

$$\mathbf{M_g}\ddot{\mathbf{u}} + \mathbf{C_g}\dot{\mathbf{u}} + \mathbf{K_g}\mathbf{u} = \mathbf{F} \tag{6}$$

where $\mathbf{M_g}$ and $\mathbf{C_g}$ are the combined system mass and damping matrices respectively, $\mathbf{K_g}$ is the coupled time-varying system stiffness matrix and $\mathbf{F}$ is the system force vector. The vector, $\mathbf{u} = \{\mathbf{y_v}, \mathbf{y_b}\}^\mathbf{T}$ is the displacement vector of the system. The equations for the coupled system are solved using the Wilson-Theta integration scheme.[46,47] The optimal value of the parameter θ = 1.420815 is used for unconditional stability in the integration schemes.[48] The scanning frequency used for all simulations is 1000 Hz.

Concept of subtracting axle accelerations

To illustrate the concept of subtracting axle accelerations to remove the influence of the road profile, simulations are carried out using a two quarter-car model. The vehicle is represented by a pair of two-degree-of-freedom unconnected quarter-cars (with identical properties), as illustrated in Figure 1. The spacing between each quarter-car is 2 m. They travel at a constant identical speed of 20 m s^{-1}, giving a constant spacing.

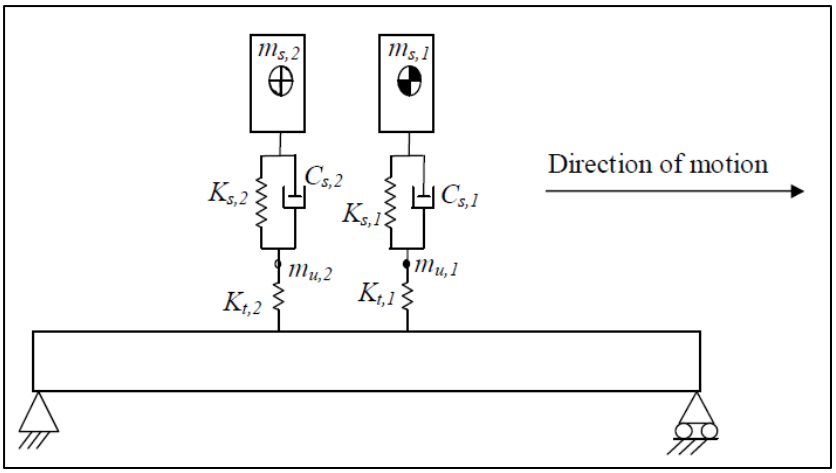

Figure 1. Two Identical Quarter-Cars.

The properties of the two identical quarter-cars are listed in Table 1. All property values are based on values gathered from the literature.[35,40,49]

Table 1. Quarter-car Properties.

Property	**Symbol**	**Value**	**Unit**
Body Mass	$m_{s,1}$, $m_{s,2}$	10 000	kg
Axle masses	$m_{u,1}$, $m_{u,2}$	700	kg
Suspension stiffness	$K_{s,1}$, $K_{s,2}$	4×10^5	N m^{-1}
Suspension Damping	$C_{s,1}$, $C_{s,2}$	10×10^3	Ns m^{-1}
Tyre Stiffness	$K_{t,1}$, $K_{t,2}$	1.75×10^6	N m^{-1}
Moment of Inertia	$I_{s,1}$, $I_{s,2}$	53 651	kg m^2
Body bounce frequency	$f_{body,1}$, $f_{body,2}$	0.9405	Hz
Axle hop frequency	f_{axle1}, f_{axle2}	8.8321	Hz

The displacement vector of the vehicle is $\mathbf{y_v} = \{y_{s,1},\ y_{u,1},\ y_{s,2},\ y_{u,2},\}^{\mathrm{T}}$. The vector $\mathbf{f_v}$ contains the time varying interaction forces applied by the two quarter-cars to the bridge, $\mathbf{f_v} = \{0 \quad -F_{t,1} \quad 0 \quad -F_{t,2}\}^{\mathrm{T}}$. The term $F_{t,i}$ represents the dynamic interaction force at wheel *i*:

$$F_{t,i} = K_{t,i}(y_{u,i} - y_{br,i} - r_i); \qquad i = 1,2 \tag{7}$$

It follows from Table 1 that the static axle loads of the vehicle are P_1 = P_2 = 98,080 N. The equations of motion of the VBI model are shown below. The four degrees of freedom correspond to body bounce (equation (8)) and axle hop for each quarter-car (equation (9)).

$$m_{s,i}\ddot{y}_{s,i} + C_{s,i}(\dot{y}_{s,i} - \dot{y}_{u,i}) + K_{s,i}(y_{s,i} - y_{u,i}) = 0; \qquad i = 1,2 \tag{8}$$

$$m_{u,i}\,\ddot{y}_{u,i} - C_{s,i}(\dot{y}_{s,i} - \dot{y}_{u,i}) - K_{s,i}(y_{s,i} - y_{u,i}) - P_i + F_{t,i} = 0; \qquad i = 1,2 \tag{9}$$

The two quarter-cars (Figure 1) are simulated crossing a 100 m approach length followed by a 15 m simply supported bridge, both containing the Class 'A' road profile[50] of Figure 2.

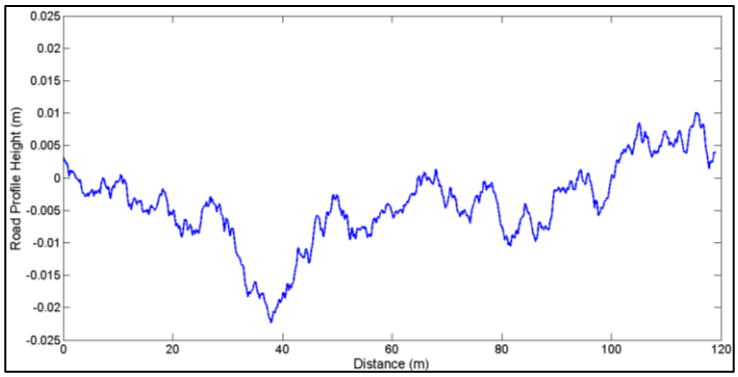

Figure 2. Class 'A' Road Profile.[50]

This is repeated six times, once for each level of damping (from 0% to 5%). From the same simulations, the bridge displacements under the 1st and 2nd axle (one curve for each level of bridge damping) are plotted in Figure 3(a). These plots are distance-referenced, i.e., each axle displacement is plotted against its distance from the start of the bridge. As the axles arrive on the bridge at different instants in time, the plots are 'time lagged' by the inter-arrival time, i.e., for any given distance, Axle 2 corresponds to a later

time than Axle 1. The total displacement is an oscillation about the static response. The time lag causes differences in the responses. For example, as Axle 2 arrives on the bridge, it is already deflecting under Axle 1 (which is 2 m in from the support).

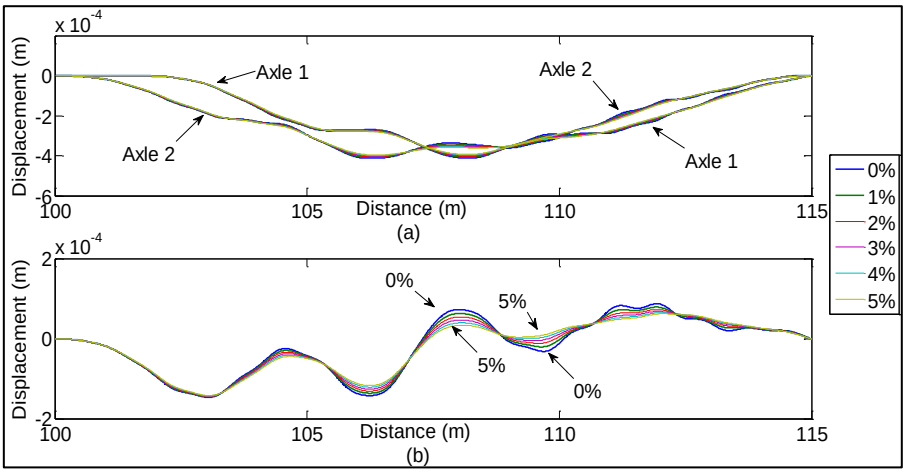

Figure 3. Bridge Displacements; (a) Bridge Displacement Experienced by each Axle (b) Difference in Bridge Displacements Experienced by each Axle.

Axle 1 is excited by the road profile and the bridge displacements as it passes each point on the bridge. Axle 2 is excited by the same road profile and bridge displacements at different instants in time. The differences between the displacement excitations, illustrated in Figure 3(b), include no element of road profile, only consisting of time lagged differences in bridge displacement. As such, this difference plot can be used to identify the influence of the bridge alone, without 'contamination' from the excitations due to road surface profile. It follows that the effect of bridge damping, hardly visible in Figure 3(a), is clearly evident in Figure 3(b). Due to the principle of linearity,[37] the quarter car accelerations due to the differences in excitations (i.e., due to the profile of Figure 3(b)) must equal the differences in the Axle 1 and Axle 2 quarter car accelerations. This has been confirmed by numerical simulation. A single quarter-car is simulated crossing the simply supported bridge with the profile of Figure 3(b). The simulation is repeated six times, once for each level of damping, and the results illustrated in Figure 4. The resulting

accelerations are an exact match to the difference in accelerations between Axles 1 and 2 (Figure 3(a)). As the influence of road profile has been removed, the influence of bridge damping is clearly visible in Figure 4.

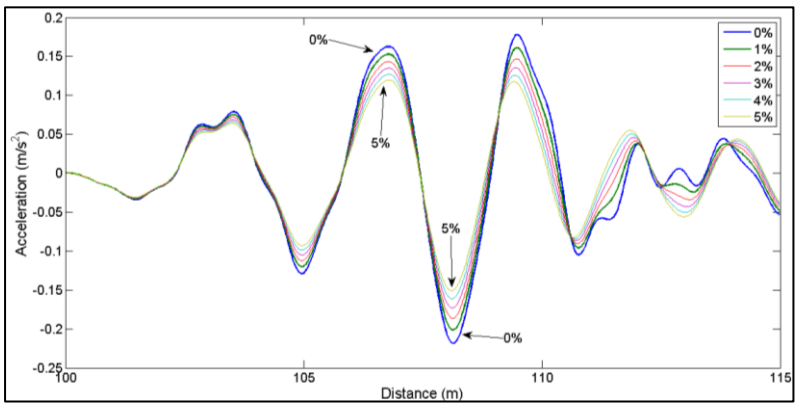

Figure 4. Time-Lagged Differences in Quarter-Car Accelerations while Travelling over the Bridge with a Road Profile.

The quarter-car accelerations are transformed from the time domain into the frequency domain using the Fast Fourier Transform. The six different PSD curves are plotted on the same graph and can be seen in Figure 5.

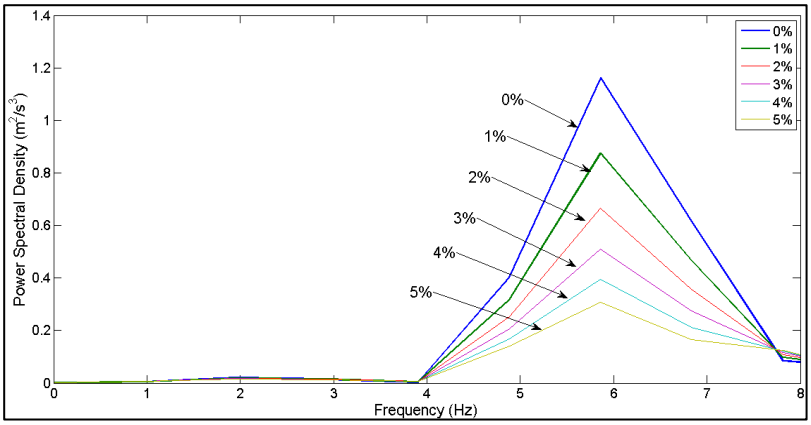

Figure 5. PSD of Acceleration difference for Vehicle Travelling at 20 m s^{-1} over a 15 m Beam with Rayleigh damping.

Peaks in the acceleration spectra can be seen in Figure 5 near the bridge frequency (5.65 Hz). A pronounced decrease in PSD peak can be seen as bridge damping increases.

Rational for the use of Rayleigh damping

This paper aims to detect a change in damping which may be used as a warning sign that a bridge is becoming unsafe, rather than accurately assessing the source of damping. While the use of damping alone as a damage indicator may not provide conclusive information about damage, when it is used together with environmental measurements and frequencies, it can be used as a reference to prioritise those bridges that need further attention.

Hysteresis damping – an alternative model to rayleigh damping

The true damping characteristics of structures are complex and difficult to define. To determine the effect of other damping models on the performance of the technique the damage detection algorithm was applied to acceleration signals that had been simulated with a hysteresis damping model. Given that hysteresis damping is defined in terms of energy loss per cycle, and is a nonlinear function of displacement amplitude, it does not readily lend itself to analytical solution. However, a viscous-type damping formulation is quite conducive to mathematical analysis. Therefore for convenience of analysis, hysteresis damping can be defined as an equivalent viscous damping coefficient.[47]

Results from VBI modelling with five different levels of damping, modelled with hysteresis damping, yield the power spectral density plots seen in the Figure 6. When Figure 6 is compared to Figure 5, it can be seen that the performance of the technique appears identical and the Rayleigh damping model and Hysteresis damping model yield the same results in this case.

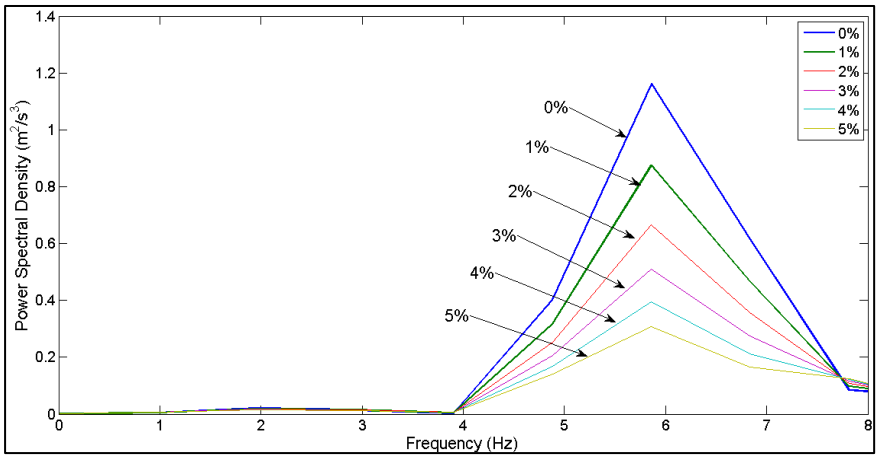

Figure 6. PSD of Acceleration difference for Vehicle Travelling at 20 m s^{-1} over a 15 m Beam with Hysteresis damping.

Comparison with a case where damage modelled as a loss in stiffness

Damage is modelled as a triangulated loss in stiffness as recommended by Sinha et al.[51] The crack causes a loss in stiffness over a region of three times the beam depth varying linearly for a maximum at the centre. A damage parameter, δ, is defined as the ratio of crack depth to overall beam depth; thus δ = 0.2 implies that the crack depth is 20% of the beam depth. Damage parameters varying from 0 to 0.5 in increments of 0.1 are investigated here. An Eigen-analysis is preformed and the eigenvalues (frequencies) are extracted. The change in frequency expected for each crack size is shown in Table 2.

Table 2. Expected frequency for each crack size.

Crack size (% of beam depth)	Frequency (Hz)
0%	5.65
10%	5.53
20%	5.40
30%	5.26
40%	5.11
50%	4.97

The axle accelerations are subtracted from one another, allowing for the time shift. Peaks are visible at 5.86 Hz (Figure 7), corresponding to the first natural frequency of the beam, 5.65 Hz.

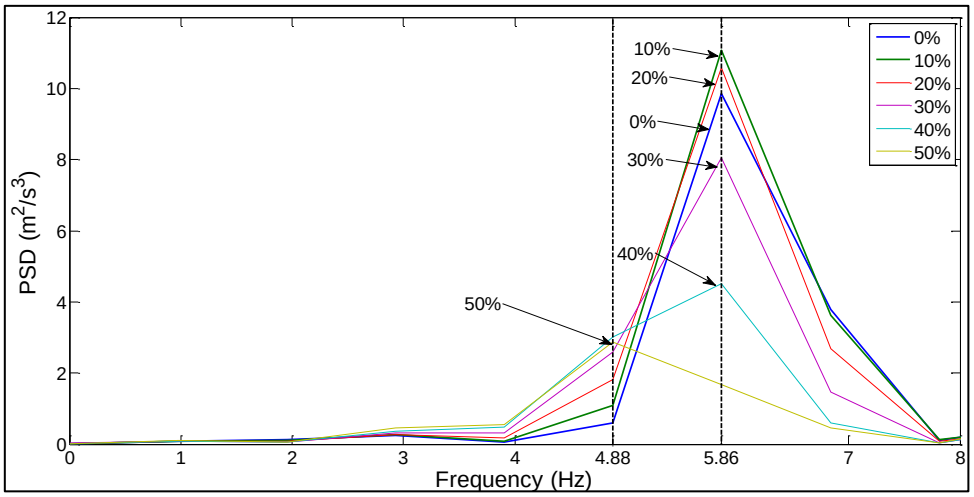

Figure 7. PSD of Acceleration difference for Vehicle Travelling at 20 m s^{-1} over a 15 m Beam with damage modelled as a loss in stiffness.

Given the spectral resolution (± 0.48 Hz), Figure 7 illustrates that it is not possible to distinguish between the frequencies at different damage levels for a vehicle speed of 20 m s^{-1}. The peaks corresponding to crack sizes of 0% - 40% of beam depth (at 5.86 Hz) do not yield a detectable change in frequency. Also, the peaks appear out of order and so it is not possible to use the PSD as an indicator of damage here.

Attempts were made to improve the spectral resolution. Once above a threshold frequency (of twice the Nyquist frequency to be detected), changing the scanning frequency will not yield a better resolution, and in this model, a scanning frequency of 1000 Hz is more than sufficient. The only way of improving the frequency resolution of the signal is to increase the time-length of the signal (i.e. increasing the length of time the vehicle is on the bridge). This can be done by reducing the speed of the vehicle. The truck-trailer now travels at a speed of 1 m s^{-1} over the 15 m beam. The trailer axle accelerations are subtracted from one another and changes in the frequency peaks now become visible as seen in Figure 8.

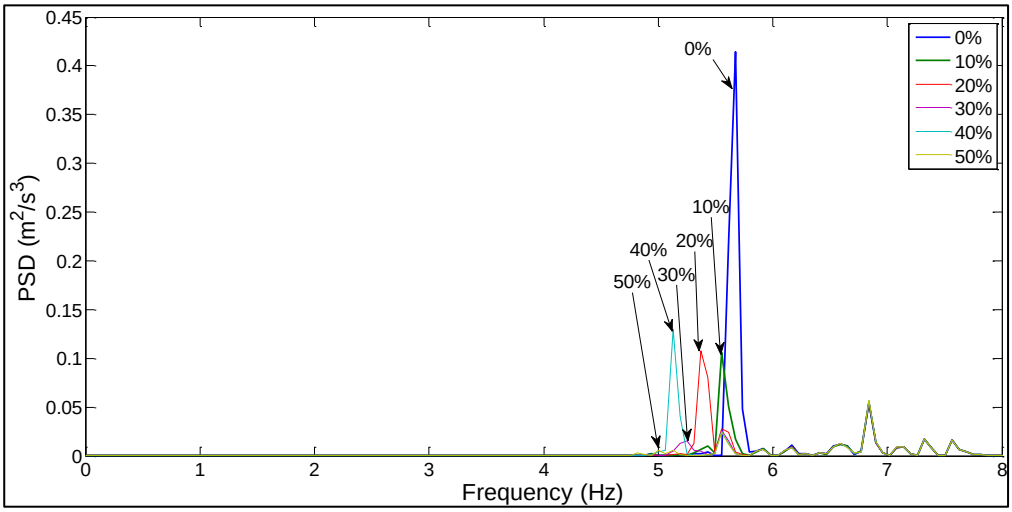

Figure 8. PSD of Acceleration difference for Vehicle Travelling at 1 m s^{-1} over a 15 m Beam with damage modelled as a loss in stiffness.

The frequencies at which each of the peaks appears in Figure 8 have been extracted and along with the expected peaks, previously calculated, are shown in Table 3. There is good agreement between them.

Table 3. Comparison of expected peaks and peaks from Figure 8.

Crack size (% of beam depth)	Expected Frequency (Hz)	Frequency from Fig. 8 (Hz)
0%	5.65	5.676
10%	5.53	5.554
20%	5.40	5.371
30%	5.26	5.249
40%	5.11	5.127
50%	4.97	5.005

The drawback of using frequency in 'Drive-by bridge inspection' as a damage indicator, compared with damping, is that the vehicle must be travelling very slowly - less than 1 m s^{-1} in order to detect the change, as there are issues with spectral resolution. The issue of spectral resolution does not arise with the use of damping as a damage indicator.

Use of a truck-trailer vehicle model to detect changes in bridge damping

A truck-trailer model (Figure 9) is now used to represent the vehicle in simulations. The truck is a three axle, five-degree-of-freedom suspension model. The five degrees-of-freedom account for the axle hop displacements of each of the three axles, $y_{u,i}$ $(i = 1,2,3)$, sprung mass bounce displacement, $y_{s,1}$, and sprung mass pitch rotation, $\theta_{s,1}$. The body of the vehicle is represented by the sprung mass, $m_{s,1}$, and the axle components are represented by the unsprung masses, $m_{u,1}$, $m_{u,2}$and $m_{u,3}$respectively. The axle masses connect to the road surface via springs of stiffness $K_{t,1,}$ $K_{t,2}$ and $K_{t,3}$, while the body mass is connected to the tyres by springs of stiffness $K_{s,1}$, $K_{s,2}$ and $K_{s,3}$ with viscous dampers of value $C_{s,1}$, $C_{s,2}$ and $C_{s,3}$. This combination represents the suspension of the truck system.

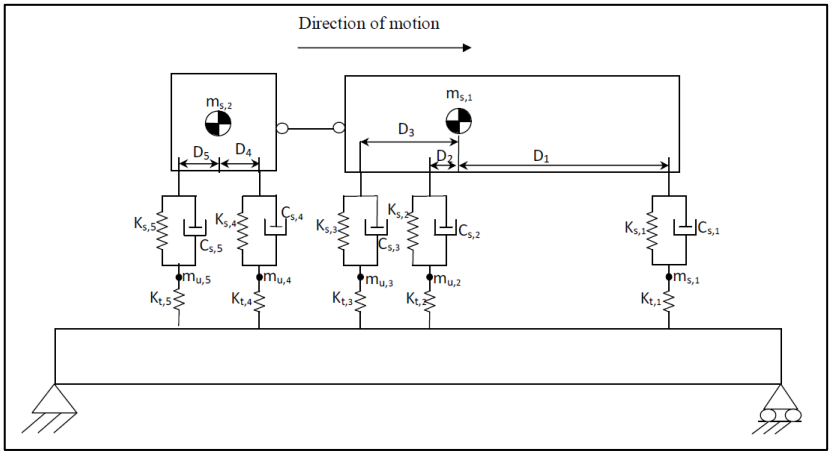

Figure 9. Truck-Trailer Model.

The trailer is a two axle, four-degree-of-freedom half-car suspension model. The four degrees-of-freedom account for axle hop displacements of each of the two axles, $y_{u,i}$ $(i = 4,5)$, sprung mass bounce displacement, $y_{s,2}$ and sprung mass pitch rotation, $\theta_{s,2}$. The body of the vehicle is represented by the sprung mass, $m_{s,2}$, and the axle components are represented by the unsprung masses, $m_{u,4}$ and $m_{u,5}$. The suspension springs have stiffness $K_{t,4}$ and $K_{t,5}$, while the tyres springs have stiffness $K_{s,4}$ and $K_{s,5}$. The viscous dampers have coefficients, $C_{s,4}$ and $C_{s,5}$. Tyre damping is assumed to be negligible here for both

the tractor and trailer and is thus omitted. The model also accounts for the sprung mass moments of inertia $I_{s,1}$ and $I_{s,2}$for the truck and trailer respectively. The centre of gravity of the truck is taken to be at two thirds the wheel base length from the front axle, and the centre of gravity of the trailer is taken to be central between the axles. The vector $\mathbf{f_v}$ contains the time varying interaction forces applied by the vehicle to the bridge: $\mathbf{f_v} = \{0 \quad 0 \quad -F_{t,1} \quad -F_{t,2} \quad -F_{t,3} \quad 0 \quad 0 \quad -F_{t,4} \quad -F_{t,5}\}^{\mathrm{T}}$. The truck and trailer vehicle properties are gathered from the literature [31, 36, 51] and presented in Table 4. The geometry and mass of the truck are obtained from a manufacturer specification for a 30 t three-axle truck.[52]

Table 4. Truck and Trailer Properties.

Property	Unit	Truck Symbol	Truck Value	Trailer Symbol	Trailer Value
Body Mass	kg	$m_{s,1}$	27100	$m_{s,2}$	400
Axle masses	kg	$m_{u,1}$	700	$m_{u,4}$	50
		$m_{u,2}$	1100	$m_{u,5}$	50
		$m_{u,3}$	1100		
Suspension stiffness	N m^{-1}	$K_{s,1}$	4×10^5	$K_{s,4}$	4×10^5
		$K_{s,2}$	1×10^6	$K_{s,5}$	4×10^5
		$K_{s,3}$	1×10^6		
Suspension Damping	Ns m^{-1}	$C_{s,1}$	10×10^3	$C_{s,4}$	10×10^3
		$C_{s,2}$	20×10^3	$C_{s,5}$	10×10^3
		$C_{s,3}$	20×10^3		
Tyre Stiffness	N m^{-1}	$K_{t,1}$	1.75×10^6	$K_{t,4}$	1.75×10^6
		$K_{t,2}$	3.5×10^6	$K_{t,5}$	1.75×10^6
		$K_{t,3}$	3.5×10^6		
Moment of Inertia	kg m^2	$I_{s,1}$	1.56×10^5	$I_{s,2}$	241.67
Distance of axle to centre of gravity	m	D_1	4.57	D_4	1
		D_2	1.43	D_5	1
		D_3	3.23		
Body mass frequency	Hz	$f_{body,1}$	1.12	$f_{body,2}$	1.77
Axle mass frequency	Hz	$f_{axle,1}$	8.84	$f_{axle,4}$	33.1
		$f_{axle,2}$	10.18	$f_{axle,5}$	33.1
		$f_{axle,3}$	10.22		

The equations of motion of the vehicle are obtained by imposing equilibrium of all forces and moments acting on the vehicle and expressing them in terms of degrees of freedom as seen in equation (5). The equations of motion of the VBI model are shown below. The nine degrees of freedom correspond to body bounce of the truck (equation (10)) and trailer (equation (11)), body pitch of the truck (equation (12)) and trailer (equation (13)), and axle hop for each of the five axles; the latter can be represented by the form given in equation (14). The term $F_{t,i}$ represents the dynamic interaction force at wheel *i* given by equation (7).

$$m_{s,1}\ddot{y}_{s,1} + C_{s,1}(\dot{y}_{s,1} + D_1\dot{\theta}_{s,1} - \dot{y}_{u,1}) + K_{s,1}(y_{s,1} + D_1\theta_{s,1} - y_{u,1}) + C_{s,2}(\dot{y}_{s,1} - D_2\dot{\theta}_{s,1} - \dot{y}_{u,2}) + K_{s,2}(y_{s,1} - D_2\theta_{s,1} - y_{u,2}) + C_{s,3}(\dot{y}_{s,1} - D_3\dot{\theta}_{s,1} - \dot{y}_{u,3}) + K_{s,3}(y_{s,1} - D_3\theta_{s,1} - y_{u,3}) = 0 \quad (10)$$

$$m_{s,2}\ddot{y}_{s,2} + C_{s,4}(\dot{y}_{s,2} + D_4\dot{\theta}_{s,2} - \dot{y}_{u,4}) + K_{s,4}(y_{s,2} + D_4\theta_{s,2} - y_{u,4}) + C_{s,5}(\dot{y}_{s,2} - D_5\dot{\theta}_{s,2} - \dot{y}_{u,5}) + K_{s,5}(y_{s,2} - D_5\theta_{s,2} - y_{u,5}) = 0 \quad (11)$$

$$I_{s,1}\ddot{\theta}_{s,1} + D_1\left[C_{s,1}(\dot{y}_{s,1} + D_1\dot{\theta}_{s,1} - \dot{y}_{u,1}) + K_{s,1}(y_{s,1} + D_1\theta_{s,1} - y_{u,1})\right] - D_2\left[C_{s,2}(\dot{y}_{s,1} - D_2\dot{\theta}_{s,1} - \dot{y}_{u,2}) + K_{s,2}(y_{s,1} - D_2\theta_{s,1} - y_{u,2})\right] - D_3\left[C_{s,3}(\dot{y}_{s,1} - D_3\dot{\theta}_{s,1} - \dot{y}_{u,3}) + K_{s,3}(y_{s,1} - D_3\theta_{s,1} - y_{u,3})\right] = 0 \quad (12)$$

$$I_{s,2}\ddot{\theta}_{s,2} + D_4\left[C_{s,4}(\dot{y}_{s,2} + D_4\dot{\theta}_{s,2} - \dot{y}_{u,4}) + K_{s,4}(y_{s,2} + D_4\theta_{s,2} - y_{u,4})\right] - D_5\left[C_{s,5}(\dot{y}_{s,2} - D_5\dot{\theta}_{s,2} - \dot{y}_{u,5}) + K_{s,5}(y_{s,2} - D_5\theta_{s,2} - y_{u,5})\right] = 0 \quad (13)$$

$$m_{u,i}\ddot{y}_{u,i} - C_{s,i}\left(\dot{y}_{s,j} \pm D_i\dot{\theta}_{s,j} - \dot{y}_{u,i}\right) - K_{s,1}\left(y_{s,j} \pm D_i\theta_{s,j} - y_{u,i}\right) - P_i + F_{t,i} = 0; \quad i = 1,2,\dots,5; j = 1,2 \quad (14)$$

In equation (14), for i = 1, 4, $D_i\dot{\theta}_{s,j}$ is taken as a positive number, and for i = 2, 3, 5, $D_i\dot{\theta}_{s,j}$ is taken as negative.

Detecting changes in damping using the truck-trailer model

The aim of this paper is to determine if changes in bridge damping, which would indicate damage in a bridge, can be detected using the truck-trailer system. The use of the PSD of vehicle acceleration differences is investigated as an indicator of changes in damping. If changes in PSD can be detected when changes in bridge damping occur, this would suggest that the approach could be used as a damage detection tool.

The PSD of the trailer axle accelerations for the vehicle system travelling at 20 m s^{-1} over a 15 m bridge are illustrated in Figure 10. In the PSD's for individual axles of the trailer (Figure 10(a) and 10(b)), there is no peak corresponding to the bridge frequency (5.65 Hz) and there is no clear distinction between the different levels of damping (all six plots are on top of one another). The vibration of the vehicle dominates each spectrum. This is because the ratio of height of road irregularities to bridge displacements is too large for the bridge to have a significant influence on the vehicle.

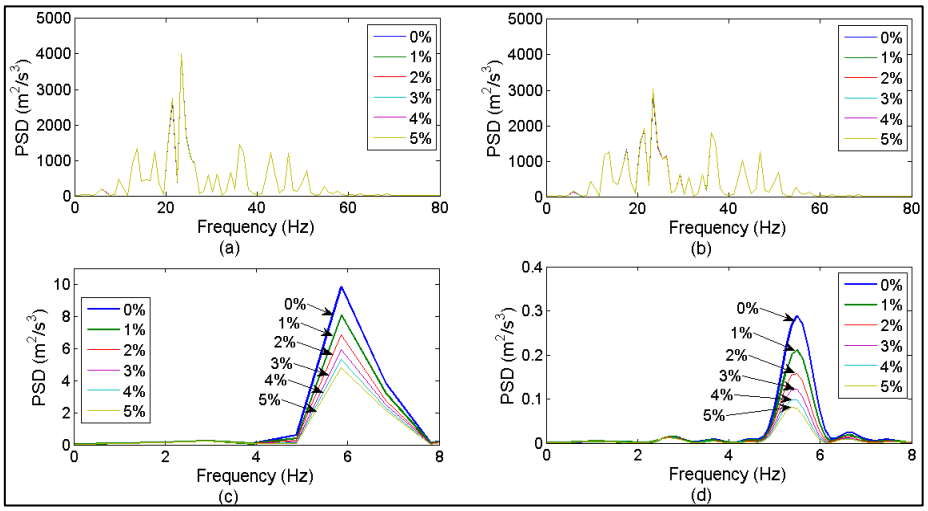

Figure 10. PSD of Accelerations for Vehicle Travelling at 20 m s^{-1} over a 15 m Bridge; (a) Axle 1 Accelerations (b) Axle 2 Accelerations (c) Axle Acceleration Difference (d) Beam Midspan Accelerations.

However, when the trailer axle accelerations are subtracted from one another, allowing for the time shift, clear peaks become visible corresponding to the first natural frequency of the bridge, seen in Figure 10(c). The PSD of the bridge midspan accelerations can be seen in Figure 10(d). This is the acceleration reading from instrumentation of the bridge as opposed to the vehicle. The peaks in Figure 10(c) and 10(d) both occur at 5.86 Hz and are similarly distinct. This suggests that instrumentation of the vehicle can be of similar accuracy to results found by instrumenting the bridge. There is a small difference between the frequencies that were predicted (5.65 Hz) and where the peak occurs (5.86 Hz) in Figure 10. The inaccuracy appears to be due to the spectral resolution (± 0.48 Hz), which can be improved by driving the vehicle at a slower speed. Also, it is apparent that the magnitude of the peak decreases for higher levels of damping. In effect, as with the earlier simpler example, the subtraction of accelerations removes the influence of the road profile. This suggests that a truck-trailer vehicle system has the potential to be a practical method of detecting changes in PSD which then may be used as an indicator of changes in bridge damping.

Effectiveness of the algorithm in the absence of noise

This section assesses the sensitivity of the algorithm to vehicle speed, road profile roughness and bridge span length. To investigate the sensitivity to vehicle speed, the bridge span is kept constant at 15 m and an ISO Class A 'very good' road profile is used in simulations. The vehicle speeds investigated here are 14 m s^{-1}, 20 m s^{-1} and 28 m s^{-1}. Figure 11 shows the sensitivity of the peak PSD to changes in damping ratio.

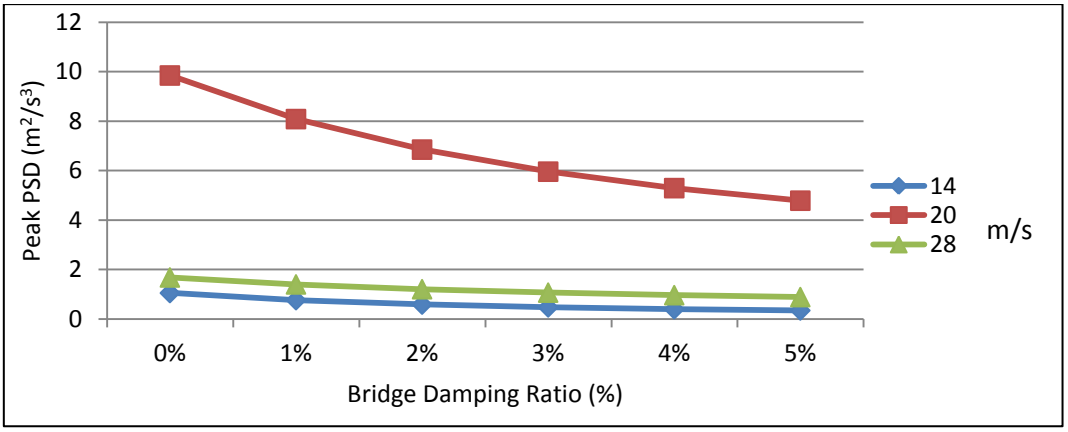

Figure 11. Change in Peak PSD to a 1% Decrease in Damping Ratio for a 15 m Bridge, Road Profile Class 'A' and for Three Vehicle Speeds.

For example, for the vehicle speed of 20 m s^{-1}, the decrease in peak PSD between 0% and 1% bridge damping ratio levels can be seen in Figure 10 to be 1.8 m^2 s^{-3}. For each of the vehicle speeds, there is a decrease in PSD as the bridge damping increases. This is an important result as it suggests that PSD may be used as an indicator of changes in bridge damping. A clear trend can also be seen for each of the vehicle speeds – the PSD is more sensitive to changes in damping for lower levels of bridge damping and less effective for highly damped bridges. For the examples considered, sensitivity is greatest for the typical highway speed of 20 ms^{-1}. This may be the result of a link between bridge natural frequency, inter-axle gap and speed, which would imply that certain speeds are more effective than others for a given bridge.

The road profile roughness is varied in simulations to assess the sensitivity of the algorithm to a change in road profile roughness class. The irregularities of this profile are randomly generated according to the ISO standard.[49] Three profile types are considered; from a Class 'A' road (very good profile, as expected in a well maintained highway), to a Class 'C' road (average profile). Other randomly generated road profiles were tested in simulations but were found to have no effect on the effectiveness of the approach

and so these results are omitted. The geometric spatial means of the Class 'A', 'B' and 'C' profiles are 16 × 10^{-6} (m^3 $cycle^{-1}$), 64 × 10^{-6} (m^3 $cycle^{-1}$) and 256 × 10^{-6} (m^3 $cycle^{-1}$) respectively. A 100 m approach length is included in each road profile prior to the bridge. The vehicle speed is kept constant in these simulations at 20 m s^{-1} and the bridge span is kept constant at 15 m. Figure 12 shows the peak PSD values for bridge damping ratios between 0% and 5%. In general, the absolute changes in peak PSD that result from changes in damping are greater when the road is rougher but the percentage changes are greater when it is smoother. It would appear that a rough road profile is more effective at exciting the bridge but that the rougher profiles do introduce inaccuracies in the accelerations, perhaps due to rocking motions in the trailer.

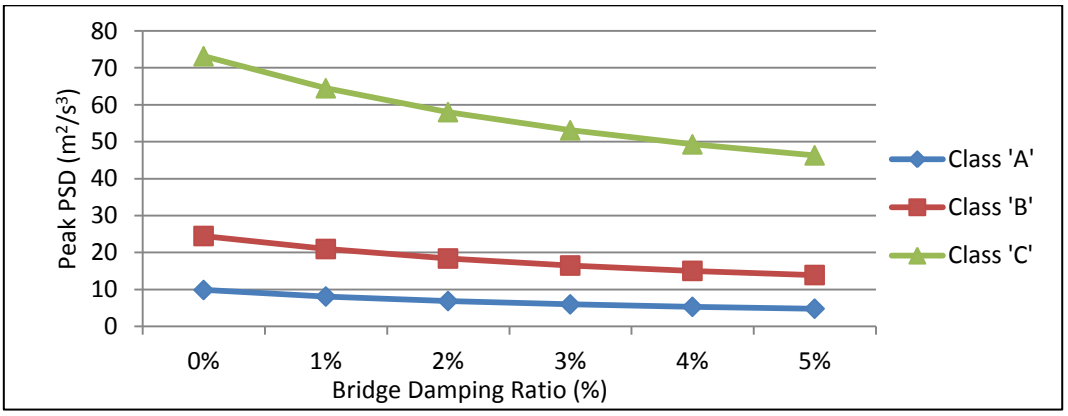

Figure 12. Peak PSD as a function of Bridge Damping, for Road Roughness Classes 'A', 'B' and 'C' for a Vehicle Travelling at 20 m s^{-1} over a 15 m Bridge.

A sensitivity analysis for bridge span length is also carried out using the same simply supported FE beam model described in the section titled '*Vehicle model*'. The bridge span length is varied in simulations from 10 m, 15 m, 20 m to 25 m to assess the sensitivity of the approach to a change in bridge span. The 10 m, 15 m and 20 m bridge models have a T-beam cross-section and the 25 m bridge model has a Y-beam cross-section. For this investigation, the vehicle speed is kept constant at 20 m s^{-1} and an ISO Class A 'very good' road profile is included in simulations. A similar trend was found as for the change in vehicle

speeds and changes in road profile roughness. Changes in peak PSD were detected for changes in damping for each of the bridge spans investigated. In general, the peak PSD is more sensitive to changes in damping for shorter bridge spans although the differences are not large.

Implications of white noise in accelerations

The issue of random noise has been addressed by many researchers. Zhu and Law[53] add 1%, 5% and 10% random noise to simulated strain signals from a beam in a moving load identification problem to represent random errors. The noise-corrupted signal is the sum of the original signal plus the noise. Noise is calculated in that study as the product of the percentage of noise to be added, the standard deviation of the signal and a standard normal distribution vector with zero mean and unit standard deviation. Zhu and Law[54] add 1%, 3% and 5% noise to beam displacements in a wavelet-based crack identification algorithm to generate the noisy signal and, in another study[55] add 1%, 5% and 10% noise to strain and displacement signals for a damage detection algorithm. All three papers calculate the noise in the same manner. González et al.[56] add 2% noise to strain signals in a Moving Force Identification (MFI) algorithm where the noise is calculated as a percentage of maximum strain. Hester and González[57] and González et al.[58] add 5% and 3% noise to accelerations of a beam and a vehicle respectively, to simulate corrupted measurements with the noise calculated as a percentage of the standard deviation of the signal.

In this paper, Additive White Gaussian Noise (AWGN) is added to the acceleration signals. It is assumed that there are two measurement sources obtained as input for the algorithm. Noise is added to the signals according to equation (15) [59] ;

$$A_{polluted} = A + E_{noise} * Noise \quad (15)$$

where $A_{polluted}$ is the acceleration signal containing noise, A is the original acceleration signal containing no noise, *var(A)* is the variance of the acceleration signal, *Noise* is a standard normal distribution vector with zero mean and unit standard deviation and E^2_{noise} is the square of the energy in the noise. The term, E^2_{noise}, is determined from the definition of the *SNR* given by equation (16):

$$SNR = 10\ log_{10} \frac{var\ (A)}{E_{noise}^2} \quad (16)$$

which is the ratio of the power in the signal to the power in the noise. In these simulations, the *SNR* is specified, and *var (A)* is easily determined. A profilometer (a vehicle fitted with accelerometers that is used to measure road profiles) is used to study signal noise. A noise signal was measured and plotted in Figure 13.

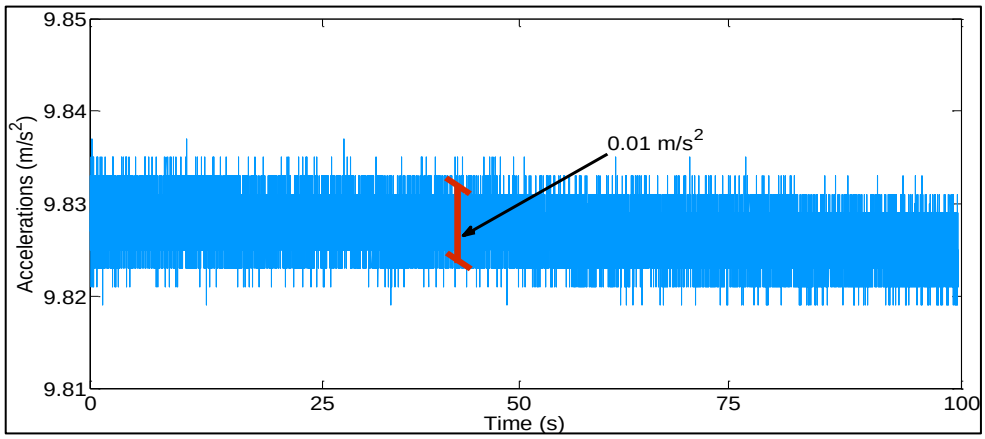

Figure 13. Noise signal measured using a profilometer.

As can be seen, the measured signal varied about a mean by ±0.005 m s^{-1}. Using Eq. (16), noise at an *SNR* level of 50 is added in this paper (which corresponds to the recorded noise level).

Sensitivity of results to noise

The vehicle was simulated travelling at 14 m s^{-1}, 20 m s^{-1} and 28 m s^{-1} across a 15 m bridge containing an ISO road profile of Class 'A' to see if the algorithm was sensitive to changes in speed with the presence of 2% noise. The same trend was found as Figure 9 without noise and so the figure has been omitted here. This is important as it suggests that the PSD may be used as an indicator of changes in bridge damping even when noise is present in the signal.

Figure 14 shows the sensitivity of the peak PSD to damping for different levels of road roughness, in the presence of 2% measurement noise.

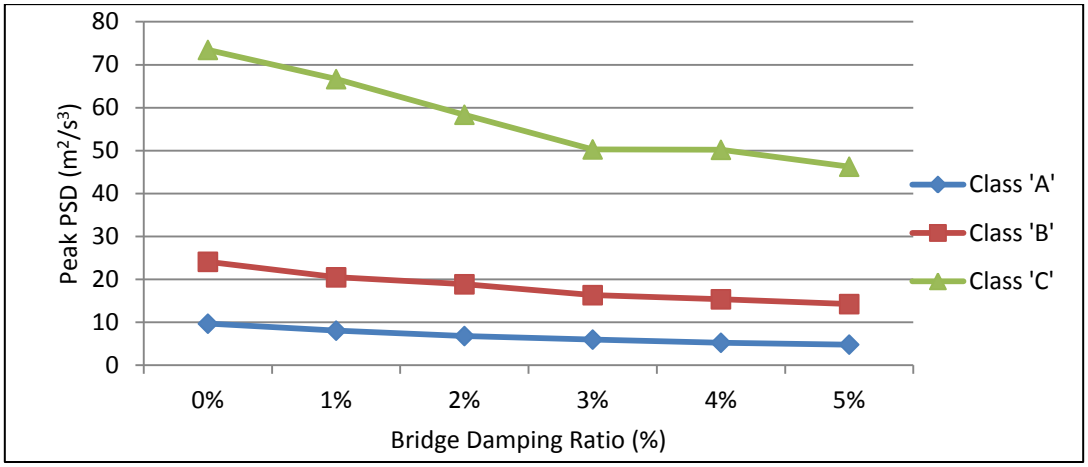

Figure 14. Peak PSD as a Function of Bridge Damping for Road Roughness Classes 'A', 'B' and 'C' for a Vehicle Travelling at 20 m s^{-1} over a 15 m Bridge, in the presence of 2% measurement noise.

The changes in PSD in the acceleration difference signal are influenced by the presence of noise. Although a falling trend may be seen for the Class 'C' road profile; it is not reliable. For this example, the peak PSD does not change when bridge damping falls from 3% to 4%. Figure 15 shows the sensitivity of the peak PSD to damping for four different bridge spans, in the presence of 2% measurement noise.

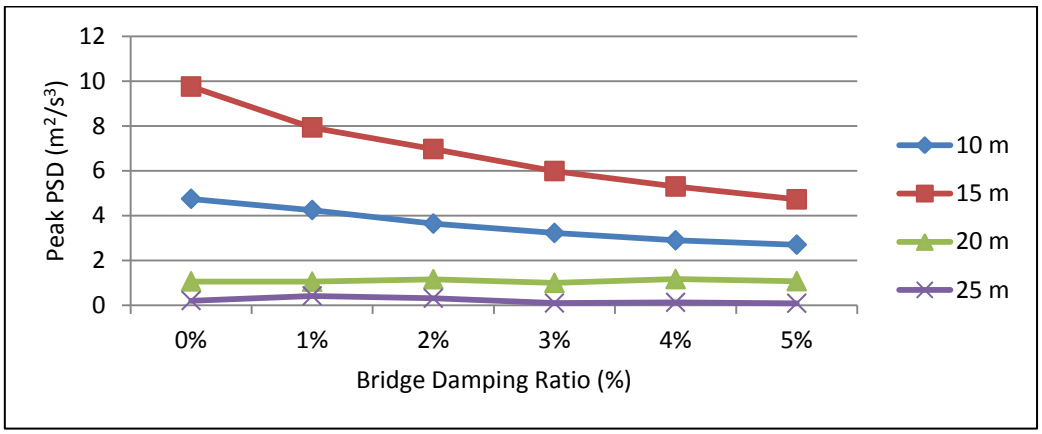

Figure 15. Peak PSD Points for each Level of Damping, for a Vehicle Travelling at 20 m s^{-1} over a Road Profile Class 'A' for Four Bridge Spans, in the presence of 2% measurement noise.

It can be seen that the approach works for the shorter spans (10 m and 15 m) although the trend is not consistent (15 m is better than both 10 m and 20 m). The insensitivity for longer spans may be because the vehicle mass remains constant throughout the simulations as the bridge span increases. As a result, the vehicle to bridge mass ratio decreases with increasing span, resulting in less excitation of the bridge. Thus, as it appears that this approach is less effective for longer bridge spans and it may be beneficial to use a heavier vehicle when implementing the approach with those spans.

Monte Carlo simulation, sampling from a normal distribution, is used to generate a population of fifty vehicle models with 10% noise (SNR = 10) in overall properties combined with 0.5% noise (SNR = 200) in the differences between axle properties. The axle properties that are investigated are the axle mass, suspension stiffness, suspension damping and tyre stiffness. Each of these fifty truck-trailer models is simulated crossing over the same 15 m simply supported beam. The mean peak PSD of the fifty simulations, for each level of bridge damping, is plotted in Figure 16. An 'error bar' is added of ± one standard deviation. The error bars have been shifted slightly from their true x-axis position so that they can be distinguished from one another. This is repeated for 1% noise (SNR = 100) change in difference of axle properties.

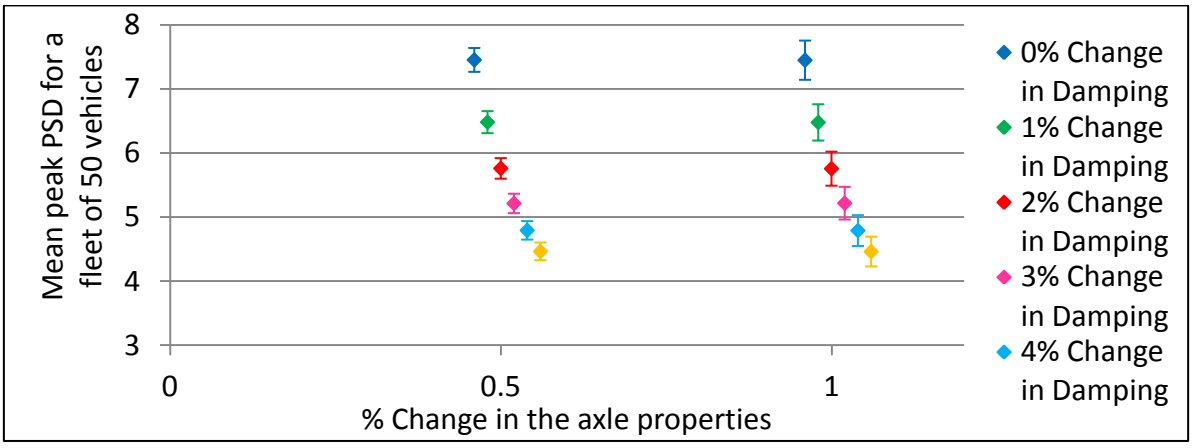

Figure 16. Mean ± one standard deviation of the peak PSD points for a fleet of fifty truck-trailer vehicle models with 10% noise in the overall axle properties with 0.5% and 1% noise in differences in properties

between axles. The error bars have be shifted slightly from their true x-axis position so that they can be distinguished from one another.

Results indicate that damage can be detected quite effectively for a 0.5% change in differences in axle properties, in the presence of 10% noise in the overall vehicle properties, while the method is less effective for a 1% difference in axle properties.

Conclusions

This paper investigates the feasibility of using an instrumented truck-trailer vehicle model to monitor damping in a bridge. A method is presented that involves the subtraction of axle accelerations to remove much of the influence of the road profile. The results indicate that bridge frequency and changes in damping can be detected when the axle accelerations of the trailer are subtracted from one another. Results for the drive-by system are of similar quality to results for an accelerometer located on the bridge. This is the case for a range of vehicle speeds, road profile classes and bridge spans when the spectra contain no added noise. When 2% Additive White Gaussian Noise is added to the simulation data, the results are less consistent. Both Rayleigh damping and hysteresis damping models are tested in simulations and results are found be similar for both. However, it is found to be difficult to detect damage, modelled as a loss in stiffness, from changes in frequency using this approach due to spectral resolution. Simulations results indicate that the approach is more effective for the monitoring of damping in shorter bridges. Overall, the results presented in the paper indicate that the method has the potential to be developed as an effective tool for the monitoring of bridge damping.

Acknowledgements

The authors wish to express their gratitude for the financial support received from Science Foundation Ireland towards this investigation under the US-Ireland Research Partnership Scheme.

References

1. Brownjohn JMW. Structural health monitoring of civil infrastructure. *Philos. Trans. R. Soc. London, Ser. A* 2007; 365: 589-622.
2. Chang PC, Flatau A and Liu SC. Review paper: health monitoring of civil infrastructure. *Structural Health Monitoring* 2003; 2: 257-267.
3. Farrar CR and Worden K. An introduction to structural health monitoring. *Philos. Trans. R. Soc. London, Ser. A* 2007; 365: 303-315.
4. Kim CW and Kawatani M. Challenge for a drive-by bridge inspection. In: Proceedings of the Tenth International Conference on Structural Safety and Reliability, Osaka, Japan, 2009, pp. 758-765.
5. Salawu OS. Detection of structural damage through changes in frequency: a review. *Eng. Struct.* 1997; 19: 718-723.
6. Carden EP and Fanning P. Vibration based condition monitoring: a review. *Structural Health Monitoring* 2004; 3: 355-377.
7. Yang YB, Lin CW and Yau JD. Extracting bridge frequencies from the dynamic response of a passing vehicle. *J. Sound Vib.* 2004; 272: 471-493.
8. Lin CW. and Yang YB. Use of a passing vehicle to scan the fundamental bridge frequencies: An experimental verification. *Eng. Struct.* 2005; 27: 1865-1878.
9. Yang YB and Chang KC. Extraction of bridge frequencies from the dynamic response of a passing vehicle enhanced by the EMD technique. *J. Sound Vib.* 2009; 322: 718-739.
10. Oshima Y, Yamaguchi T, Kobayashi Y, et al. Eigenfrequency estimation for bridges using the response of a passing vehicle with excitation system. In: Proceedings of the Fourth International Conference on Bridge Maintenance, Safety and Management, Seoul, Korea, 2008, pp. 3030-3037.
11. Cerda F, Garrett J, Bielak J, et al. Indirect structural health monitoring in bridges: scale experiments. In: Proceedings of the Sixth International Conference for Bridge Maintenance and Safety, 2012, Stresa, Italy, pp. 346-353.
12. Toshinami T, Kawatani M and Kim CW. Feasibility investigation for identifying bridge's fundamental frequencies from vehicle vibrations. In: Proceedings of the Fifth International Conference on Bridge Maintenance, Safety and Management, USA, 2010, pp. 317-322.
13. Curadelli RO, Riera JD, Ambrosini D, et al. Damage detection by means of structural damping identification. *Eng. Struct.* 2008; 30: 3497-3504.
14. González A, Rattigan P, OBrien EJ, et al. Determination of bridge lifetime dynamic amplification factor using finite element analysis of critical loading scenarios. *Eng. Struct.* 2008; 30: 2330-2337.
15. Yabe A and Miyamoto A. Bridge condition assessment for short and medium span bridges by vibration responses of city bus. In: Proceedings of the Sixth International Conference for Bridge Maintenance and Safety, 2012, Stresa, Italy, pp. 195-202.
16. Kim CW, Isemoto R, Sugiura K, et al. Structural diagnosis of bridges using traffic-induced vibration measurements. In: Proceedings of the Sixth International Conference for Bridge Maintenance and Safety, 2012, Stresa, Italy, pp. 423-430.
17. Williams C and Salawu OS. Damping as a damage indication parameter. In: Proceedings of the 15th International Modal Analysis Conference, 1997, Orlando, Florida, USA, pp. 1531-1536.
18. Wahab MA and De Roeck G. Effect of Temperature on Dynamic System Parameters of a Highway Bridge. *Structural Engineering International* 1997; 7: 266-270.
19. Modena C, Sonda D and Zonta D. Damage localization in reinforced concrete structures by using damping measurements. *Key Eng. Mater.* 1999; 167: 132-141.

20. Gutenbrunner G, Savov K and Wenzel H. Sensitivity studies on damping estimation. In: Proceedings of the Second International Conference on Experimental Vibration Analysis for Civil Engineering Structures, Porto, Portugal, 2007.
21. Jeary AP. The description and measurement of nonlinear damping in structures. *J. Wind Eng. Ind. Aerodyn.* 1996; 59: 103-114.
22. Kawiecki G. Modal damping measurement for damage detection. *Smart Mater. Struct.* 2001; 10: 446-471.
23. Brady SP and OBrien EJ. Effect of vehicle velocity on the dynamic amplification of two vehicles crossing a simply supported bridge. *J. Bridge Eng.* 2006; 11: 250-256.
24. Brady SP, OBrien EJ and Znidaric A. Effect of vehicle velocity on the dynamic amplification of a vehicle crossing a simply supported bridge. *J. Bridge Eng.* 2006; 11: 241-249.
25. Savin E. Dynamic amplification factor and response spectrum for the evaluation of vibrations of beams under successive moving loads. *J. Sound Vib.* 2001; 267-288.
26. Green MF, Cebon D and Cole DJ. Effects of vehicle suspension design on dynamics of highway bridges. *J. Struct. Eng.* 1995; 121: 272-282.
27. Yang YB and Lin BH. Vehicle-bridge interaction analysis by dynamic condensation method. *J. Struct. Eng.* 1995; 121: 1636-1643.
28. Yang YB and Chang KC. Extracting the bridge frequencies indirectly from a passing vehicle: Parametric study. *Eng. Struct.* 2009; 31: 2448-2459.
29. Yang YB and Yau JD. Vehicle-bridge interaction element for dynamic analysis. *J. Struct. Eng.* 1997; 123: 1512-1518.
30. Green MF and Cebon D. Dynamic response of highway bridges to heavy vehicle loads: theory and experimental validation. *J. Sound Vib.* 1994; 170: 51-78.
31. Li Y, OBrien EJ and González A. The development of a dynamic amplification estimator for bridges with good road profiles. *J. Sound Vib.* 2006; 293: 125-137.
32. McGetrick PJ, González A and OBrien EJ. Theoretical investigation of the use of a moving vehicle to identify bridge dynamic parameters. *Insight: Non-Destructive Testing & Condition Monitoring* 2009; 51: 433-438.
33. Seetapan P and Chucheepsakul S. Dynamic response of a two-span beam subjected to high speed 2dof sprung vehicles. Int. *J. Struct. Stab. Dyn.* 2006; 6: 413-430.
34. Yang YB, Chang CH and Yau JD. An element for analysing vehicle–bridge systems considering vehicle's pitching effect. *Int. J. Numer. Methods Eng.* 1999; 46: 1031-1047.
35. Cebon D. *Handbook of Vehicle-Road Interaction*. The Netherlands: Swets & Zeitlinger, 1999.
36. Kim CW, Kawatani M and Kim KB. Three-dimensional dynamic analysis for bridge-vehicle interaction with roadway roughness. *Comput. Struct.* 2005; 83: 1627-1645.
37. OBrien EJ, Li Y and González A. Bridge roughness index as an indicator of bridge dynamic amplification. *Comput. Struct.* 2006; 84: 759-769.
38. Cantero D, OBrien EJ and González A. Modelling the vehicle in vehicle infrastructure dynamic interaction studies. *Proceedings of the Institution of Mechanical Engineers, Part K: Journal of Multi-body Dynamics* 2010; 224: 243-248.
39. González A, Covián E and Madera J. Determination of bridge natural frequencies using a moving vehicle instrumented with accelerometers and a geographical positioning system. In: Proceedings of the Ninth International Conference on Computational Structures Technology, Athens, Greece, 2008, Paper 281.
40. Harris NK, OBrien EJ and González A. Reduction of bridge dynamic amplification through adjustment of vehicle suspension damping. *J. Sound Vib.* 2007; 302: 471-485.
41. Nassif HH and Liu M. Analytical modeling of bridge-road-vehicle dynamic interaction system. *J. Vib. Control* 2004; 10: 215.

42. OBrien EJ, Cantero D, Enright B, et al. Characteristic dynamic increment for extreme traffic loading events on short and medium span highway bridges. *Eng. Struct.* 2010; 32: 3827-3835.
43. Deng L and Cai CS. Development of dynamic impact factor for performance evaluation of existing multi-girder concrete bridges. *Eng. Struct.* 2010; 32: 21-31.
44. Yang YB, Yau JD and Wu YS. *Vehicle-Bridge Interaction Dynamics: with Applications to High-Speed Railways*. Singapore: World Scientific Publishing Co. Pte. Ltd, 2004.
45. Clough RW and Penzien J. *Dynamics of structures*, McGraw-Hill, 1975.
46. Bathe KJ and Wilson EL. *Numerical methods in finite element analysis*, Prentice-Hall, 1976.
47. Tedesco JW, McDougal WG and Ross CS. *Structural dynamics: theory and applications*, Addison Wesley Longman, 1999.
48. Weaver W and Johnston PR. *Structural dynamics by finite elements*, Prentice-Hall, 1987.
49. A. González, E.J. O'Brien, P.J. McGetrick, Detection of bridge dynamic parameters using an instrumented vehicle, Proceedings of the Fifth World Conference on Structural Control and Monotoring, Tokyo, Japan, 2010, Paper 34.
50. ISO 8608. Mechanical vibration-road surface profiles - reporting of measured data, 1995.
51. Sinha JK, Friswell MI and Edwards S. Simplified Models for the Location of Cracks in Beam Structures Using Measured Vibration Data. *J. Sound Vib.* 2002; 251: 13-38.
52. DAF Trucks Limited, FAT CF75 30t Specification sheet, 2012.
53. Zhu XQ and Law SS. Orthogonal Function in Moving Loads Identification in a Multi-span Bridge. *J. Sound Vib.* 2001; 245: 329-345.
54. Zhu XQ and Law SS. Wavelet-based crack identification of bridge beam from operational deflection time history. *Int. J. Solids Struct.* 2006; 43: 2299-2317.
55. Zhu XQ and Law SS. Damage detection in simply supported concrete bridge structure under moving vehicular loads. *J. Vib. Acoust.* 2007; 129: 58-65.
56. González A, Rowley C and OBrien EJ. A general solution to the identification of moving vehicle forces on a bridge. *Int. J. Numer. Methods Eng.* 2008; 75: 335-354.
57. Hester D and González A. A wavelet-based damage detection algorithm based on bridge acceleration response to a vehicle. *Mech. Syst. Sig. Process.* 2012; 28: 145-166.
58. González A, OBrien EJ and McGetrick PJ. Identification of damping in a bridge using a moving instrumented vehicle. *J. Sound Vib.* 2012; 331: 4115-4131.
59. Lyons R. *Understanding Digital Signal Processing*, 3rd ed. Boston, Prentice-Hall, 2011.